Geo-Marine Letters (2021) 41: 41
https://doi.org/10.1007/s00367-021-00711-w

ORIGINAL

Mapping diamondiferous palaeo-shorelines in complicated terrain: seismic and GIS-based methods from the inner shelf of southern Namibia

L. H. Kirkpatrick[1] · A. N. Green[2,3]

Received: 4 November 2020 / Accepted: 11 July 2021 / Published online: 20 August 2021

Abstract

The inner shelf of Namibia's southwestern coastline comprises the submerged extension of the world's largest diamond placer deposit. The onshore raised beach deposits, which are constrained by wave-cut cliffs and platforms, bevelled into the schist bedrock during palaeo-sea level stillstands, are largely mined out. As land-based operations near their practical limit, spatially accurate resource estimation of the inner shelf becomes increasingly critical to extend the life of mine of this extensive but low-grade resource. This study analyses a comprehensive seismic-reflection dataset, to produce a 50-m cell size bedrock morphology surface for the inner shelf. The data reinforce previous results and show that inherited structural influence exerts the overarching control on bedrock morphology at the scale of the study area. However, within this framework, the detailed data have now facilitated the zonation of the study area into discrete structural zones from which subtle coast-parallel bedrock gradient changes, that we interpret to represent submerged palaeo-shoreline morphologies (i.e. bedrock gradient changes associated with wave-cut cliffs and platforms), have been extracted. These bedrock gradient variations are contextualised within areas of similar glacial isostatic adjustment (GIA) response, which lends weight to the GIS-based palaeo-shoreline interpretation. Although these may be considered composite features that are the product of 42 million years of shoreline transgression and regression, the more recent occupation of the shoreline at these depth intervals, during the late Pleistocene/Holocene, forms a critical upgrading component to the offshore resource. Our study proposes a − 20 msl shoreline, the most recent occupation of which we link to the peak of marine isotope stage (MIS) 5c, and a − 30 msl shoreline that is linked to the time shortly after MIS 5c and the peak of MIS 5a. The most recent period of shoreline occupation for the deepest shoreline at − 40 msl is attributed to slowly rising sea level between 10.8 and 10.6 ka. This information is critical to the development of the resource estimation philosophy for the offshore extension of mining operations.

Introduction

A rocky coastline's morphology is the product of the interplay of a range of forcing factors (e.g. waves, tides, sea-level change, tectonics and antecedent geologic controls) with potentially complex feedback among rock properties, weathering and erosion processes and rates and topography, at the full spectrum of temporal and spatial scale (Trenhaile, 2005, 2016; Dickson, 2006; Kennedy and Dickson, 2006; Naylor et al., 2010; Stephenson et al., 2017; Knight and Birningham, 2019; Kirkpatrick and Green, 2018). Much of the detailed study on the morphodynamic evolution of rocky shorelines aims to understand this interplay of factors on rock platform dynamics, and many different models for rocky shore platform evolution have been developed (Trenhaile 2002, 2008; Naylor et al., 2010., 2012; Matsumoto et al., 2016a). However, few detailed studies exist that apply

This article is part of the Topical Collection on *Coastal and marine geology in Southern Africa: alluvial to abyssal and everything in between*

✉ L. H. Kirkpatrick
lynette.kirkpatrick@namdeb.com

A. N. Green
greena1@ukzn.ac.za

[1] Namdeb Diamond Corporation (Pty) Ltd, PO Box 253, Oranjemund, Namibia

[2] Geological Sciences, School of Agricultural, Earth and Environmental Sciences, University of Kwazulu-Natal, Westville Campus, Private Bag X54001, Durban, South Africa

[3] Geography and Environmental Science, Ulster University, Coleraine BT52 1SA, Northern Ireland, UK

the understanding developed in these models to the detection of regional erosional palaeo-shorelines from submerged rocky coastlines, especially in cases where the bedrock is now covered in a thick sediment overburden.

The southern coast of Namibia (Fig. 1A) is host to the world's largest gem-quality diamond placer; the main economic resources of which are associated with onshore bedrock trap sites such as gullies and potholes (Fig. 1B and C). These are arranged in a topographic profile characterised by a step-like bedrock morphology (Fig1B) which is interpreted to represent wave-cut platforms and cliffs, bevelled into Late Proterozoic schists during highstands (Hallam 1964; Murray et al. 1970; Stocken 1978; Jacob et al. 2006). Their genesis is associated with a long-lived and extreme-high energy wave regime which, when combined with an abundance of large abrasive clasts supplied by the Orange River and focussed along palaeo-shorelines, carved out the characteristic wave-cut platform and cliff morphology (Jacob et al., 2006; Bluck

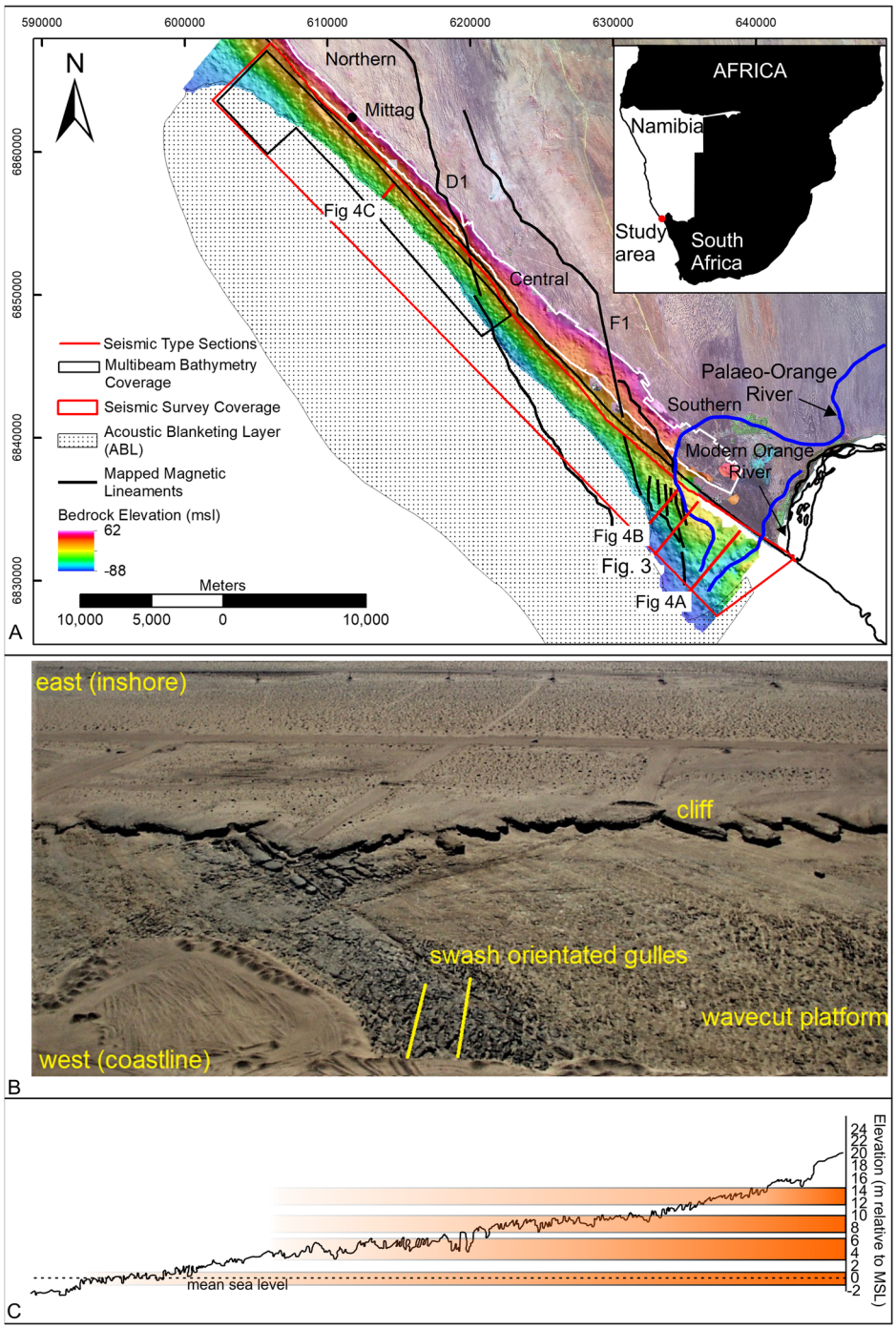

Fig. 1 Locality map (**A**) showing the seismic survey coverage that also corresponds to the offshore mining license area (red polygon), position of seismic type sections (red lines, Fig. 3), multibeam echosounder coverage (black polygon), outline of historically mapped A–F beaches (white polygon), extent of the acoustic blanketing layer (ABL) and the structural zones after Kirkpatrick and Green (2018) overlain on the bedrock elevation map derived from seismic data. **B** Aerial photograph, courtesy of Dr J. Jacob, showing the development of a marine wave-cut platform backed by ~4 m-high cliff near Mittag (as annotated on Fig. 1A). **C** Bedrock profile mapped in a historical exploration trench near Mittag. The orange banding indicates the height in relation to sea level of historically mapped wave-cut platforms that are associated with higher grade diamond deposits (after Jacob et al., 2006; Kirkpatrick et al., 2019b)

et al, 2007; Oelofsen, 2008; Kirkpatrick et al., 2019a). Kirkpatrick et al. (2019b) showed that the relative width and gradient of these raised wave-cut platforms and associated cliffs strongly influenced the diamond grades of the beaches later emplaced on them.

As mining focus in the area steadily extends into the increasingly techno-economically challenging offshore environment, mapping of similar features as those known to be diamondiferous onshore, is required. Thus, remote detection and accurate mapping of submerged wave-cut platforms and cliffs have become a critical resource estimation tool for the inner shelf of southern Namibia. Considering the absence of physical sample data to drive bankable resource estimation, high-resolution bedrock models, derived from geophysical data and coupled with GIS-based analysis, can be contextualised with a comparison to bedrock profiles onshore. With the incorporation of the diamond grades from the raised deposits, the offshore bedrock model may provide a significantly improved understanding of potential offshore diamond grade variability. This improved understanding drives the resource estimation philosophy and alleviates the regional scale risk associated with mining a marginal deposit characterised by inherent, extremely variable grade. At present, the submerged extension of the placer deposit is covered by up to 67 m of Holocene material derived from the Orange River (Kirkpatrick et al., 2019a), and thus, these important wave-cut platform and cliff features, characterised by changes of gradient in the bedrock profile, can only be detected by seismic reflection profiling. (Fig. 2)

An initial attempt to accurately map submerged wave-cut platforms and cliffs for the ~ 50 km stretch of the mining license area (Fig. 1), based on a relatively coarse 400-m-spaced seismic-reflection grid, made good headway towards achieving this goal (Kirkpatrick et al., 2019b) but did not achieve the level of spatial confidence required to support resource estimation. This current study is based on a later seismic survey, which produced data to support a 50-m cell size resource estimation. However, consistent, high resolution, line-to-line mapping of subtle erosional features (wave-cut platforms and cliffs) in a rugged, steep bedrock profile (Figs. 3 and 4) is further complicated by the macro-scale (10's of km) overprinting of the palaeo-coastlines by a series of N-S trending Neoproterozoic-age faults (Kirkpatrick and Green, 2018). The bedrock gradient variation caused by these faults obscures subtle coast perpendicular gradient variations, both along track of the individual seismic lines and at the 50-m cell size gridded scale (Fig 4C and D). Lodewyks (2010) notes similar challenges in their study of the – 114 m palaeo-shoreline, south of the Orange River where the palaeo-shoreline morphology was not evident in the gridded data.

Clear expressions of coast-parallel bedrock gradient variation related to palaeo shoreline positions are thus masked by the overall structural complexity of the site. Bedrock elevation offsets due to structural features must therefore be accounted for in a spatially accurate palaeo-shoreline mapping exercise if they are to support resource estimation for offshore mining development. The literature has widely

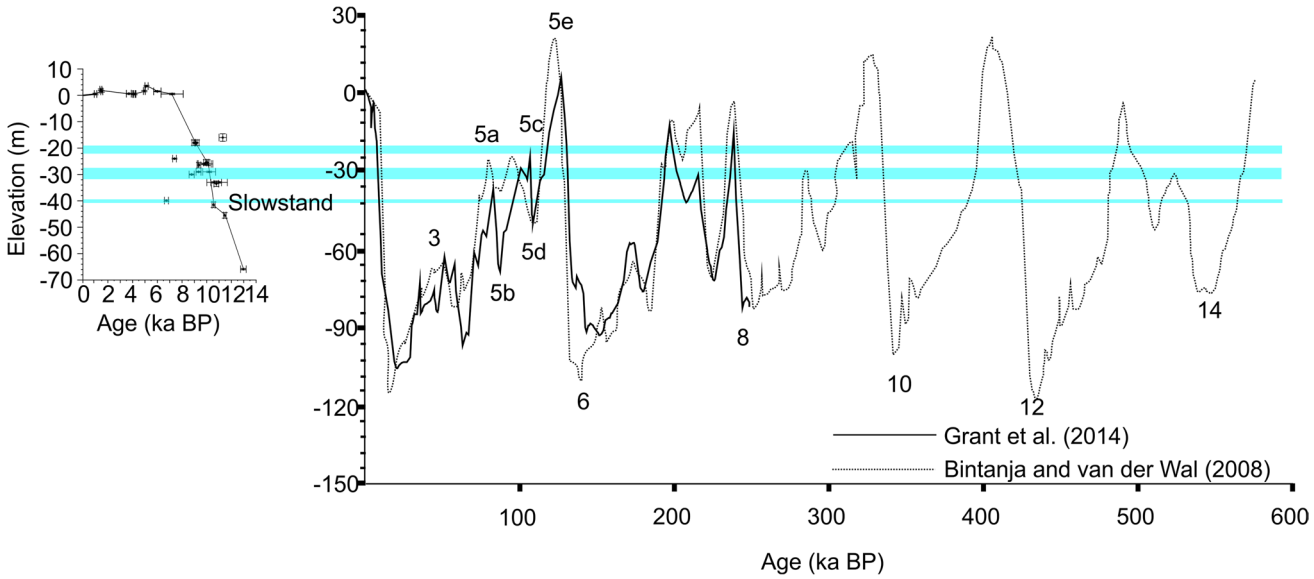

Fig. 2 Mid to late Pleistocene sea level curve (right—after Grant et al., 2014; Bintanja and van de Wal 2008) showing sea level lower than present for far greater periods of time than above present; numbers indicate marine isotope stages. On the left is the sea level curve for the east coast of South Africa (modified after Cooper et al., 2018a, b). The current west coast data do not extend as deep as the platforms mapped in this study (Cooper et al., 2018a, b) hence the use of the east coast dataset. The blue bands indicate the positions of the erosional palaeo-shorelines proposed from our dataset

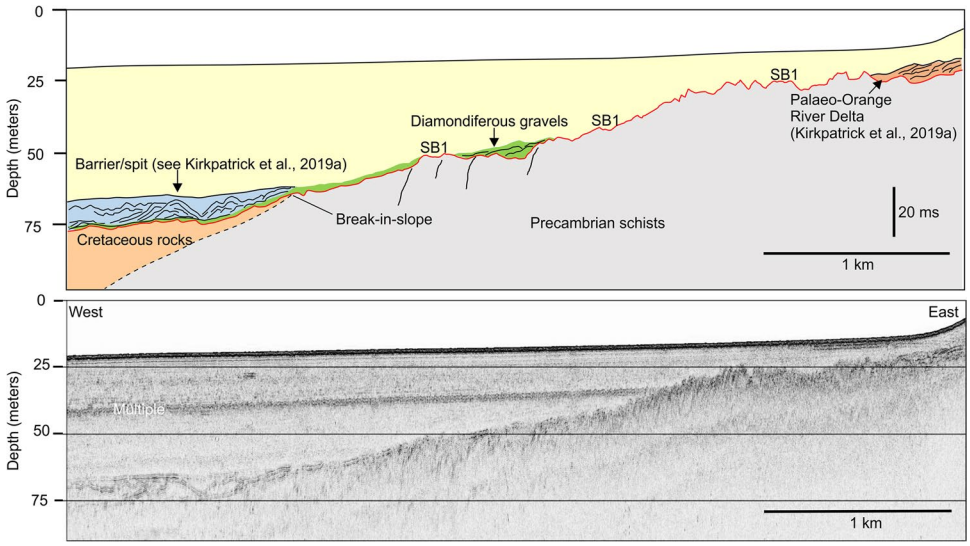

Fig. 3 Type section of the stratigraphy of the inner shelf of southern Namibia (after Kirkpatrick et al., 2019a)

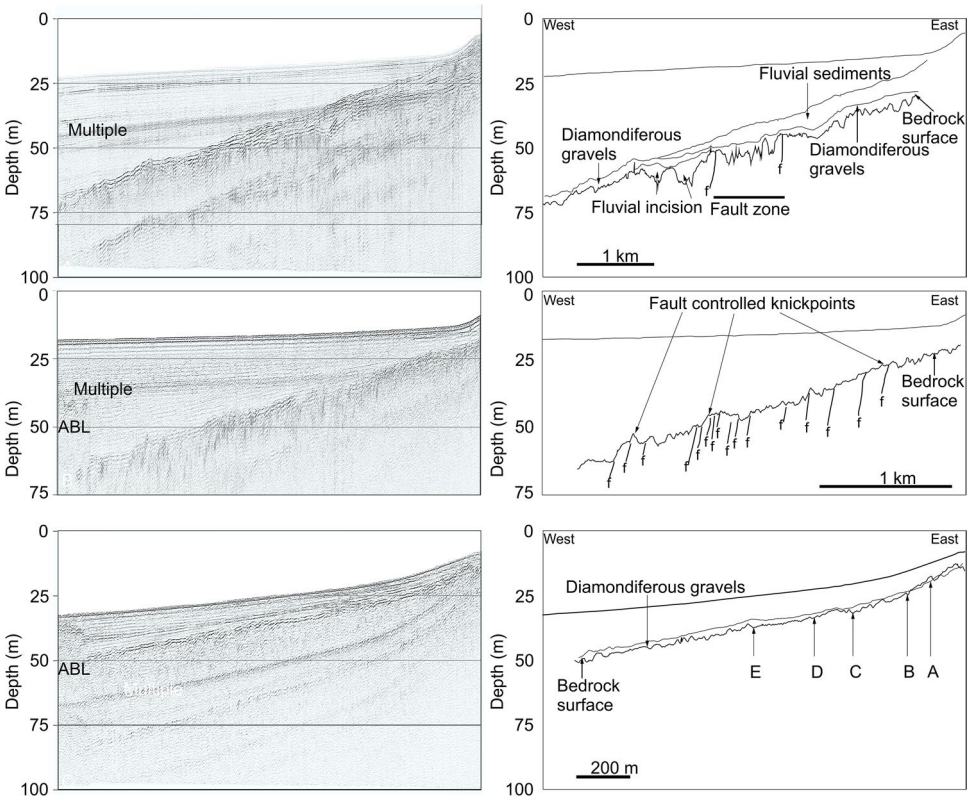

Fig. 4 Comparative bedrock profiles for the three bedrock morphology zones, with uninterpreted (left) and interpreted (right) sections. The locations of the 3 lines are shown on Fig. 1A. **A** Highly rugged bedrock horizon from SZ 1 showing fault-controlled knickpoints (characterised by parabolic reflectors in the crystalline basement lithology; faults mapped initially from magnetic data) and fluvial incisions (after Kirkpatrick and Green, 2018). The mean bedrock gradient of this profile is ~ 0.5. **B** Profile through SZ 2 showing fault-controlled knickpoints (Kirkpatrick and Green, 2018). This profile has a steep overall bedrock gradient (~ 0.9°) but it steepens at fault-controlled knickpoints (annotated) from 0.87 to 1.1° and 1.44° respectively. Maximum bedrock depth is ~ 66 msl. **C** A bedrock profile up to ~ − 50 msl in SZ6. Bedrock gradient changes are annotated at points A–E and described in detail in text

acknowledged the issue of inheritance when unravelling a shoreline signature (e.g. Thébaudeau et al., 2013), and we thus attempt to incorporate a detailed understanding of the structural inheritance of the coastline into the interpretation

of how and where expressions of submerged erosional palaeo-shorelines have developed.

In the context of this region's economic significance, this paper presents a newly revamped and more detailed bedrock morphology for the southern Namibian coastline. From this rugged and structurally controlled bedrock surface, now covered in 10's of metres of sediment, we extract subtle details that point to the existence of palaeo-shorelines with a high degree of spatial accuracy required to meet resource estimation standards. We achieve this through a GIS-based statistical approach that analyses the regions *within* structural zones, thus accounting for the influence of high magnitude bedrock gradient changes caused by structural features. We further contextualise the shoreline positions with other sites of similar glacial isostatic adjustments (GIA) and provide possible constraints on the genesis of rocky palaeo-shorelines and their relationships to lower than present sea levels.

Regional setting

Sediment supply and oceanic regime: past and present

The inner shelf of southern Namibia has been dominated by a long-lived and abundant sediment supply, sourced from the Orange River, the largest to debouch to the SW African coastline. The Orange River, which is the transport conduit of the diamonds found in the region, has drained the interior plateau of southern Africa since the Cretaceous times (Dingle and Hendey, 1984; Aizawa et al., 2000; Bluck et al., 2007). By the middle Eocene, it had superimposed its meandering form into the bedrock, fixing the mouth in approximately its present position (Jacob, 2005; Bluck et al., 2007; Kirkpatrick and Green, 2018; Fig. 1A). At present, the river debouches a predominately 'finer' load than in the past, comprising fine gravel, diamonds, sand and silt–clay onto the inner shelf. In the present coastal regime, which comprises a year-round, consistently vigorous wave regime, this load is directed towards the NE, where it fractionates and disperses northwards and westwards via strong longshore drift and subsidiary ocean currents (Rogers, 1977; Hay and Brock, 1992; Bluck et al., 2001, 2007). The coast is micro-tidal (~ 1.8 m), with a sandy nearshore submerged delta retained in the study area (Kirkpatrick et al., 2019a) and with a widespread, fine 'mud belt' to seawards and south (Rogers, 1977).

Gravels are accreted to the coastline for a distance of > 300 km north of the Orange River mouth, while the majority of the sandy material is transported northwards and alongshore for up to 700 km, where at certain points it is returned onshore to form the main Namib Sand Sea (Bluck et al., 2007). In stark contrast to the present, the river has at times carried sediment of up to boulder size to the coast (Bluck et al., 2007). In older raised beaches, cobble size clasts of known Orange River provenance have been found up to 200 km north of their entry points (Bluck et al., 2001). Ward and Bluck (1997) dated these to ~ 40 million years and demonstrated that the higher energy long-shore drift system, capable of transporting cobble sized material that distance, is particularly long-lived.

Antecedent geological control on coastline morphology

Strongly gullied and potholed Neoproterozoic chloritic schists, characterised by a N-S trending structural fabric (Fig. 1B), comprise the basement rock of the study area (Fig. 3). These form the 'footwall' of the diamond placer deposit that spans from 3 km inshore of the coastline to approximately 3 km offshore (Jacob et al., 2006; Kirkpatrick et al., 2019a). The extremely rugged nature of the bedrock is a result of swash-orientated abrasion by the coarse cobble size materials supplied by the Orange River, which are mobilised by high-energy waves to depths of ~ 15 m (Jacob et al., 2006; Bluck et al., 2007). The local-scale high rugosity of the bedrock is the primary trapping mechanism for the alluvial diamonds and is responsible for local upgrading of diamondiferous gravel to economic proportions. Understanding and estimating diamond grade variation onshore at the scale of the local bedrock rugosity using sample data has thus been the primary focus of previous work (Jacob et al., 2006; Prins and Jacob, 2014; Jacob, 2016).

Using electromagnetic and seismic reflection data, Kirkpatrick and Green (2018) documented a series of prominent faults in the bedrock. They observed relative movement along the N-S orientated faults and established that the structure divides the coastline into 3 primary zones (Fig.1A) and imposes a 1st order control on the bedrock, coastline and seafloor morphology. This spans over a 50-km-long stretch of the study area; the influence of which has persisted despite the modern high sediment supply conditions. This structural control not only extends to the creation of accommodation space and the emplacement and preservation capacity of onshore diamondiferous raised beaches (Kirkpatrick et al., 2019b), but controls (to some degree) the local wave regime responsible for the longshore transport of diamondiferous material too (Kirkpatrick and Green, 2018).

Sea level, palaeo-shoreline morphologies and diamonds

Within the regional context of the Namibian diamond mega placer, which encompasses over 300 km of the southwestern Namibian coastline and extends 10's of km offshore (Corbett and Burrell, 2001), onshore historical exploration and mining processes have revealed six main

diamondiferous raised beaches (called the "A-F" beaches, Fig.1A). These span an along-coast distance of 120 km northwards from the Orange River mouth. These beaches have been the mainstay of Namdeb Diamond Mining Corporation's (Namdeb) diamond mining activities for over 100 years. The beaches range in age and elevation from oldest, Late Pliocene to Early Pleistocene (D, E and F beaches) in the east, to the lowest elevation and youngest Mid-Pleistocene to Late Pleistocene and Holocene (C, B and A) beaches to seaward. The youngest beach is exposed at present sea level. They are emplaced on marine bevelled bedrock platforms cut in the chloritic schists, backed by cliffs of varying height (up to 3 m) on their landward edge (Hallam 1964; Corvinus 1983; Pether 1986; Jacob et al. 2006). Figure 1Band C illustrate a wave-cut platform exposed during mining operations at Mittag, a site in the north of the study area, where sediment cover is substantially less than in the south. It underlies the D, E and F beaches that contain the warm water species *Donax rogersi* and which date to between 3 and 2.5 Ma (Corvinus, 1983; Pether, 1986).

Using an extensive database of historical diamond grade and bedrock elevation information derived from the mining of these beaches, Kirkpatrick et al. (2019b) showed that the variations in bedrock gradient related to palaeo-shorelines (i.e. wave-cut cliffs vs platforms as well as steeper vs flatter platforms) are directly proportional to diamond grade within the overlying beach deposits. Placer diamond deposits are inherently low grade and characterised by extreme variability in mineralisation (Prins and Jacob, 2014; Jacob, 2016). This extreme variability necessitates a rigorous statistical resource estimation process using closely spaced sample data (Jacob, 2016). Considering the highly energetic wave regime of the nearshore, which precludes substantial physical sampling, an alternative means to quantify the controls on resource grade variability and offshore resource evaluation is required.

Over the last 40 million years, there have been substantial changes in sea level along on this coastal strip. These range from an Eocene high of ~ 180 m above present sea level to a Pleistocene low of ~ 120 m below present sea level (Fig.2, Dingle et al., 1983; Pether, 1986, 1994; Corbett, 1996). Under a more energetic climatic and oceanic regime of the past (Bluck et al., 2001, 2007), it stands to reason that lower than present sea-level stillstands would have produced at least similar, if not more distinct, erosional morphologies in the bedrock. Palaeo-shorelines should thus be more distinct or equal to those observed in the onshore environment today. Along the inner shelf to the north and south of the study area, where sediment cover is less extensive, bathymetric data have revealed wave-cut cliffs/terraces and topographic knickpoints similar in morphology to those onshore at – 20 msl, – 30 msl and – 40 msl (Murray et al., 1970; De Decker, 1987; Rau, 2003; Oelofsen, 2008).

Stratigraphy of the inner shelf of southern Namibia

The typical stratigraphy of the inner shelf of southern Namibia is provided in Fig. 3 (after Kirkpatrick et al., 2019a). The steep, rugged schist basement is onlapped by Albian-Cenomanian sedimentary units at a characteristic regional knickpoint located at approximately – 70 msl (Stevenson and McMillan 2004; Herbert 2009; Lodewyks 2010; Runds et al. 2019; Kirkpatrick 2019a). This forms the footwall to mining operations and is truncated by a subaerial unconformity (called Sequence Boundary 1, SB1, after Kirkpatrick et al., 2019a) that, in the study area, includes two palaeo-channels of the Orange River (Fig.1), incised into a fault-controlled, now submerged, palaeo-headland (Hoyt et al., 1969; Kirkpatrick and Green, 2018; Kirkpatrick et al., 2019a). A fluvial succession has been inferred within the palaeo-channels (Fig.4), and downlapping palaeo-delta deposits are noted to be preserved within the accommodation space provided by the palaeo-headland (Fig. 4) (Kirkpatrick and Green, 2018; Kirkpatrick et al., 2019b).

The footwall is draped by a diachronous, coarse diamondiferous gravel lag up to 3-m thick associated with repeated erosion events that represent multiple cycles of subaerial erosion and wave ravinement, including those of the last post-glacial transgression (Compton et al., 2002; Lodewyks, 2010; Kirkpatrick et al., 2019a). The diamondiferous horizon is overlain by a thick (up to 67 m) sandy Holocene highstand succession (Figs. 3 and 4). The Holocene sediment wedge tapers out to the north, south and offshore of the study area, where high resolution multibeam bathymetry data confirm the presence of wave-scoured, rugged bedrock on the inner shelf (Runds et al., 2019).

Methodology

Geophysical data acquisition and processing

In 2019, an Applied Acoustics 200 J boomer coupled with a 20-element towed hydrophone array was used to acquire 280 line km of new single-channel, high resolution seismic reflection data on the inner shelf of southern Namibia. When combined with boomer data acquired in 2016 and 2017, these new data effectively increased seismic coverage to 200 m line spacing over a 50 × 5 km coastal strip. Full coverage to seaward was limited due to the presence of a pervasive Acoustic Blanketing Layer (ABL) mapped by Kirkpatrick and Green (2018) (Fig. 1).

These data were processed and interpreted using the Geosuite Allworks software following the methodology

and settings as described in Kirkpatrick and Green (2018). Sequence Boundary 1 (SB1), the upper bounding horizon of the bedrock surface (mining footwall) (Kirkpatrick and Green, 2018; Kirkpatrick et al., 2019a), was digitised on each seismic section and corrected for absolute depth using a velocity of 1600 m/s and co-acquired multibeam echosounder data. The new, depth-corrected SB1 horizons were combined with the previous SB1 interpretations and merged with onshore bedrock elevations derived from historical and current mining and sampling operations. These data were gridded at a 50-m cell size, using a Minimum Curvature algorithm in Oasis Montaj, to produce a new, higher resolution onshore-offshore bedrock morphology map. Bedrock contours and a 50-m cell size bedrock gradient map were derived from the bedrock elevation map using the Spatial Analyst toolkit in ArcGIS 10.5.1, and, to support further analysis, the map was classified into 2-m contour interval polygons, each with an associated surface area.

Multibeam echosounder (MBES) data (Fig. 1) were acquired in 2015 using a Kongsberg EM710 deployed off the *MV DP Star* and processed using Qimera to a 1-m cell size grid. The data show the rugged, gullied nature of the bedrock; however, the gullies and channels are generally filled with a fining upward sequence of cobbles to fine mud material (Kirkpatrick et al., 2019a), and this creates a false smoothing of the bedrock surface in profile view. Therefore, in order to extract a bedrock elevation map unbiased by the sediment infill, the multibeam seafloor surface was classified as either bedrock or sediment, based on the morphology and backscatter properties of the seafloor. The sediment-filled areas were then removed from the bedrock to produce a seamless bedrock elevation model.

The use of the 400–1200 Hz boomer seismic system, which produces data of ~ 1.5 m vertical resolution, is not ideal for the level of detail required for mine-support mapping in this extremely rugged bedrock terrain. However, the coarseness and thickness of the overburden precludes higher resolution seismic techniques like Chirp or Topas seismic tools. Fig. 3 shows the irregularity of the bedrock horizon and highlights the difficulty of mapping bedrock knickpoints consistently from individual seismic lines. The rugged bedrock topography over the short line length (sometimes lines are as short as ~ 1.3 km due to gas blanking) further compounds consistent visual line-to-line interpretation. A more iterative and integrated approach to the data analysis was therefore required as outlined in the section below.

Bedrock morphology through area analysis

This study focuses on the inner shelf bedrock morphology at a scale and resolution that supports Namdeb's resource estimation requirements. No comparable seismic survey exists at these water depths from the region. De Decker (1987) however characterised the inner-middle shelf south of the Orange River using a 3.5 kHz echosounder where sediment cover over bedrock is thinner (< 10 m) and less extensive. His observations over an 80 km stretch of coast showed that the inner shelf morphology should be grouped into geologically similar zones, for which the dominant geological control was the type of bedrock lithology. We adopt a similar approach by identifying and analysing bedrock data within distinct geological (or structural) zones.

In each zone, we extract the surface area per a defined bedrock contour interval over 1-km-wide polygons. The surface area over a fixed width (in this case, 1 km) is indirectly proportional to bedrock gradient, and this method allowed for a simplified regional classification of bedrock gradient, which may be an indicator of wave-cut platforms and cliffs and, more importantly, a primary control of regional scale diamond grade variability over such variable terrain (Kirkpatrick et al., 2019b). Simply put, the smaller the surface area over a unit change in elevation, the steeper the bedrock gradient and the higher the diamond grades.

With modern, highly accurate positioning systems and centimetre-scale depth resolution via co-acquired multibeam data, we aim to improve on De Decker's (1987) study by producing a more detailed and spatially accurate classification in our study area. As such, smaller geological zones, all with the same bedrock lithology, were identified. We examine these data in the context of the three broad structural zones of the inner shelf previously identified by Kirkpatrick and Green (2018) (Fig. 1). This zonation is better constrained with the new seismic data set and allows for more discrete analyses regarding individual geological zones to be made.

Results

Higher resolution bedrock elevation model

Figure 5 shows the new 50-m cell size bedrock morphology map (B) in comparison to the 2018 vintage, 100-m cell size bedrock morphology map (A). Figure 6 (i, ii and iii) shows three close-up examples where detail in the bedrock morphology is very well resolved in the new 50-m cell size dataset. In particular, these three examples highlight the very prominent N-S to NNW-SSE lineaments (annotated in black) that are consistent with the structural mapping of Kirkpatrick and Green (2018), derived from magnetic data and interpreted as faults.

Figure 5 also shows the new bedrock gradient map (D) in comparison to the 2018 vintage bedrock gradient map (C). The general broad trends are evident from the 2018 gradient map, a dominant N-S to NNW-SSE, structurally controlled seafloor patterning, previously noted by Kirkpatrick et al. (2019b). With the improved data set (Fig. 6

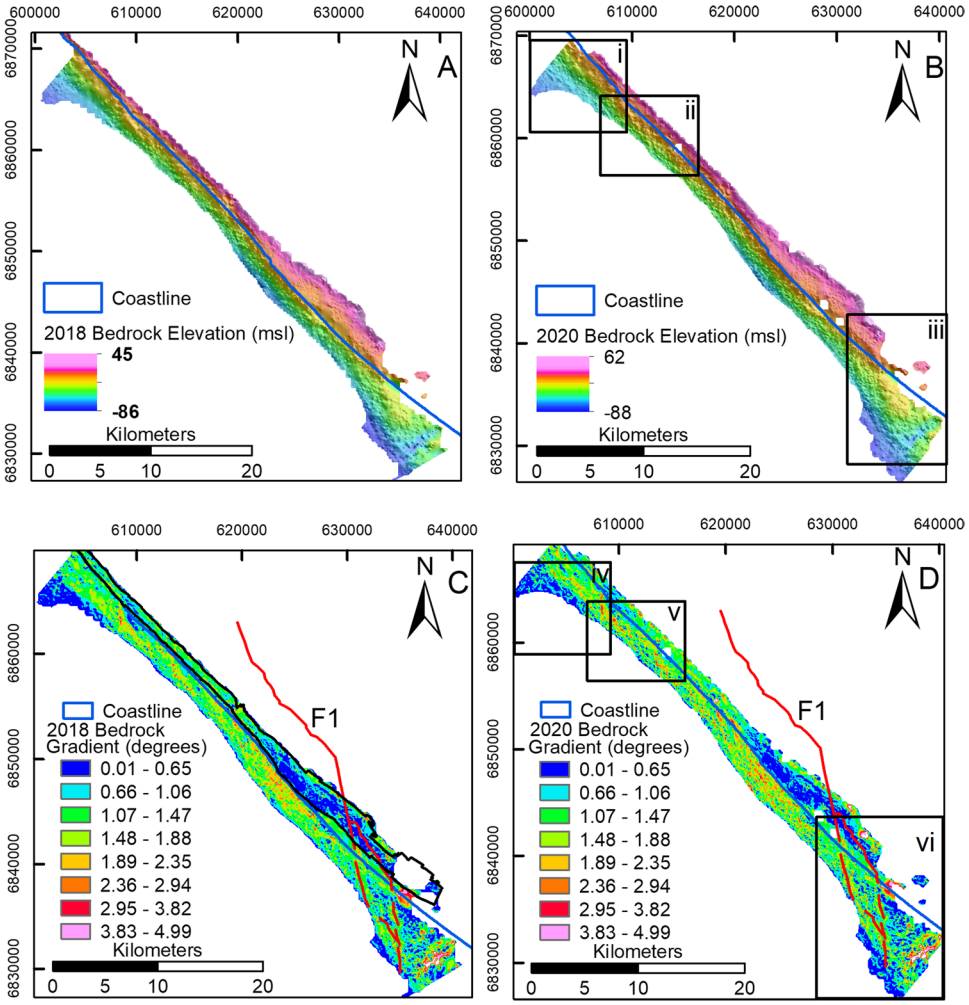

Fig. 5 Comparative bedrock morphology and gradient maps. **A** 100-m cell size, 2018 bedrock morphology map vs **B** 50-m cell size, 2020 bedrock morphology map. Inset boxes (i, ii and iii) are shown in Fig. 5. **C** 100-m cell size 2018 bedrock gradient map vs **D** 50-m cell size 2020 bedrock gradient map. Inset boxes (iv, v and vi) are shown in Fig. 6. Fault F1 of Kirkpatrick and Green (2018) is annotated in red and the outline of the onshore raised beaches exposed during historical mining operations is annotated by the black polygon in **C**

iv, v and vi), it is however now possible to map in more detail the higher gradient bedrock zones which also correspond with the structural interpretation derived from the magnetic data (Kirkpatrick and Green, 2018).

The major fault (F1) of Kirkpatrick and Green (2018) remains the dominant control on the high-gradient zones in the south (Fig. 6, vi). However, north of F1, coast-parallel high-gradient zones are now evident (Fig.6, iv and v). These coast parallel zones are not fully continuous for the length of the dataset; Fig. 6 v and vi show clear offsets of coast-parallel high-gradient zones along N-S orientated structural trends. Furthermore, although the gradient varies between 0.3 and 1.9° between the − 10 and − 50 msl isobaths, the gradient of the majority of the nearshore zone (− 10 to − 32 msl) clusters around the mean (1.33°). Thus, linking subtle variations in coast-parallel high-gradient zones across structural breaks is both visually and statistically impossible within the small range of gradient variation at the gridded resolution of the dataset.

Offshore bedrock analysis through surface area per contour interval comparison

Kirkpatrick et al. (2019b) showed that the raised A–F beaches were well-developed in an area of low gradient (0–1°), within and north of the F1 fault (Fig. 1A), and subtle increases in gradient within this low-gradient zone are directly proportional to increased diamond grades. Fig. 5C and D also show that when compared to the area where raised beaches occur, the adjacent bedrock of the nearshore zone comprises higher average gradients of between 1 and 3°. The bedrock gradient only shallows out to an average of < 1° again below ~ − 50 msl, i.e. towards the offshore edge of the survey area, which is mostly obscured by the ABL. As a result, the nearshore bedrock is typically steeper than elevated bedrock areas that host the raised diamondiferous beaches. Any gradient variations on the inner shelf that may influence diamond grade will thus occur within an overall steeper gradient zone, and as a consequence, their bedrock

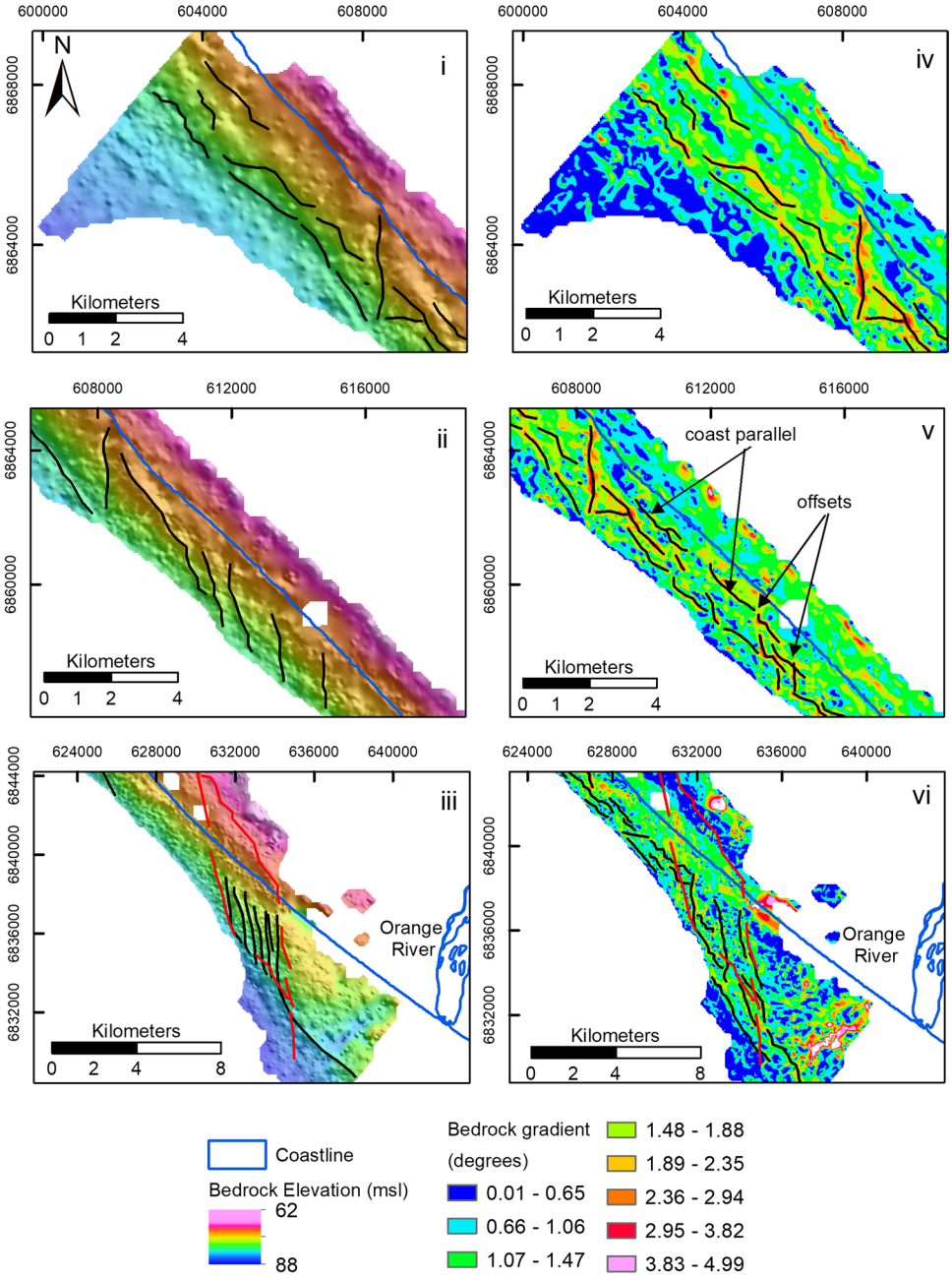

Fig. 6 Insets i to iii provide enlarged views of the updated 50-m bedrock surface derived from seismic interpretation of sequence boundary 1 (SB1). Black annotations show the increased morphology detail achieved by the infill seismic dataset. The highwater line is shown in blue and fault F1, derived from magnetic data (Kirkpatrick and Green, 2018) is annotated in red on Fig. 6iii. Insets iv, v and v provide enlarged views of the bedrock gradient map derived from the updated bedrock surface. Distinct gradient changes are newly observable, separated by multiple offsets (annotated in black). These 'offsets' make statistical extraction of the high-gradient shoreline signatures challenging

expression is likely far more subtle within this steeper context. The nearshore bedrock zone thus warrants analysis as a separate entity with our refined methodology.

Figure 7A shows the surface area per 2-m bedrock elevation contour interval for the total onshore-offshore study area. The offshore area alone is highlighted in Fig. 7B. The complete onshore-offshore data are classified into eight classes; these highlight the historical A–F beaches as a single zone (mostly pink) of natural large surface area 'similarity'. Likewise, the nearshore zone is classified as predominantly one class (red) from which no subtle detail can be extracted. When the offshore components of the data are extracted and analysed alone (Fig. 7B), more intervals of natural similarity are visible (Fig.7B inset). Intervals of natural similarity are identified between – 10 and – 20 msl (green), – 20 and – 24 msl (orange) and – 28 and – 32 msl (red). A distinct cluster, – 24 to – 28 msl and – 32 to – 50 msl, is grouped together as they comprise the highest surface area per contour interval (pink). It must be noted that total surface area per interval for the lower elevations (below – 20 msl) is not represented consistently throughout the whole offshore study area, and therefore,

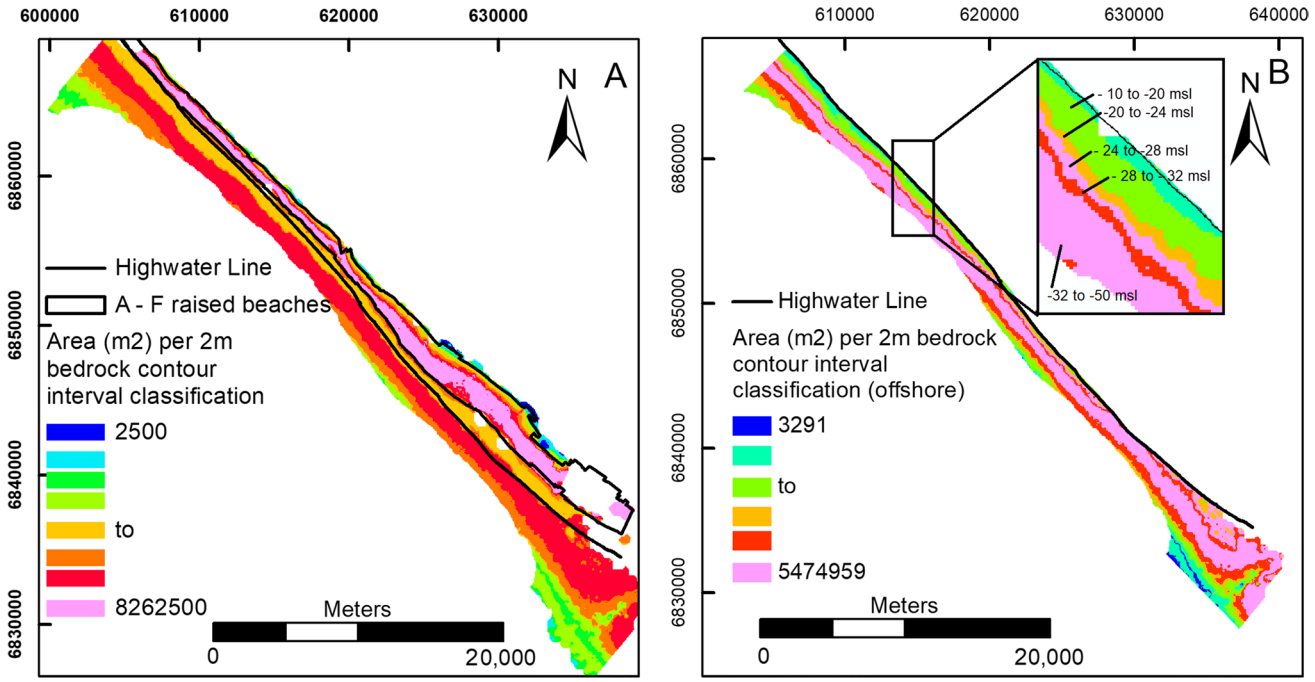

Fig. 7 Surface area per contour interval for **A** the entire onshore-offshore study area classified using a natural breaks classification (Jenks) and **B** the offshore dataset alone classified using the Natural Breaks (Jenks) classification

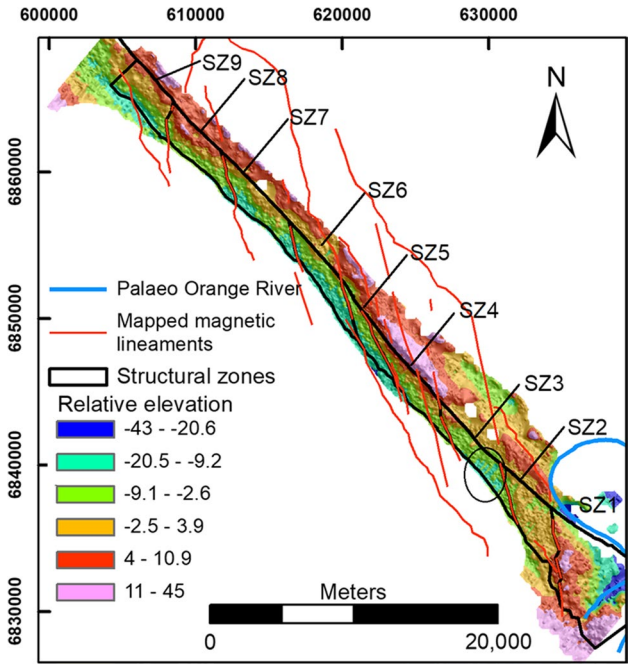

Fig. 8 Bedrock elevation map with regional gradient removed, highlighting nine structural zones (black) bounded by faults mapped from airborne magnetic data in red (Kirkpatrick and Green, 2018). Note: palaeo channels of the Orange River are annotated in blue within SZ1

these elevations have an inherent lower total surface area. For this reason, elevations lower than – 16msl have been removed from the final analysis shown in Figs. 9 and 10.

Figure 8 shows the bedrock elevation model with the regional gradient removed, overlain by previously mapped faults derived from magnetic data (Kirkpatrick and Green, 2018). Absolute elevation changes coincide with the main structural features, and this provides a basis for a better constrained set of geological zones in which more detailed interpretations can be made. Nine zones (SZ 1–9), separated by major structural features are identified. SZ 1 comprises a fluvial-incised palaeo-bedrock headland (cf. Kirkpatrick and Green, 2018). Due to a combined fluvial and structural influence (Fig. 4A), this area has a significantly different bedrock morphology to the rest of the study area and is thus excluded from the statistical analyses.

The bedrock morphology of SZ 2 is entirely fault controlled (Figs. 1 and 4B). In this zone, bedrock elevation steps steeply downwards, perpendicular to fault F1. In cross-section, the marked variability in gradient, as controlled by fault location, is clear. Gradient changes along the profile (0.87° to 1.1° to 1.44°) are associated with various fault-controlled knickpoints (Fig.4B). SZ 3 is an anomalously deep zone on the inner shelf (Fig. 8); the morphology of which is similarly controlled by dextral strike-slip motion on F1 (cf Kirkpatrick and Green, 2018). SZ 2 and SZ 3 were thus also removed from the statistical analysis.

Zones SZ 4–9 all have a broadly similar bedrock morphology, albeit at varying, fault-controlled elevations. Fig. 4C is a representative seismic section. The overall gradient of this line is 1.4°; however, local variations occur at various points (annotated). Point A (~ − 18 msl) to point B (~ − 25 msl) has a gradient of ~ 4.5°; point B to point C (~ − 32 msl) has a gradient of ~ 2°; point C to point D (~ − 35 msl) has a gradient of ~ 0.9°; point D to point E (~ − 38 msl) has a gradient of ~ 0.7°, after which the bedrock gradient dips more steeply again, but uniformly, at ~ 1.1° until the limit of the data. The influence of faults is limited to the extreme offshore end of the line where the maximum depth of bedrock is less than 50 m. As Fig.5C shows, bedrock morphology changes are subtle and, on a line-by-line basis, difficult to map objectively. On the whole however, each of these zones SZ 4–9 can be described as comprising a nearshore, coast-parallel strip of elevated bedrock gradient, followed by a uniform, coast normal bedrock slope that abruptly terminates at − 55 msl and transitions to a low-gradient (0.5–0.6°) bedrock surface (Fig. 1).

Figures 9 and 10 show the results of the surface area per m^2 per 2-m contour interval of SZ 4–SZ 9 both by individual zone (e.g. Figure 9A, C) and summed as one group (Fig.10). The analysis of individual zones produces similar but not identical values (as expected from the extremely rugged surface described above). However, the results of each zone do show overlapping trends. Fig. 9A shows the detailed analysis of SZ 6, with a four class Natural Jenks classification of the bedrock surface area over a 1-km-wide polygon between − 10 and − 48 msl. Fig. 9C shows the plot of distribution of surface area per 2-m contour interval. A larger area with a wider and flatter interval between − 20 and − 28 msl is identified, with a narrower and steeper interval at depths shallower than − 20 msl. Another steeper interval is identified between − 28 and − 32 msl, followed by an overall flatter but gradually steepening bedrock surface between − 32 and − 42 msl. The bedrock gradient flattens significantly from − 42 msl to seaward.

Figure 9B shows the 1-km-wide polygons for each structural zone. Similar trends were identified in the other zones.

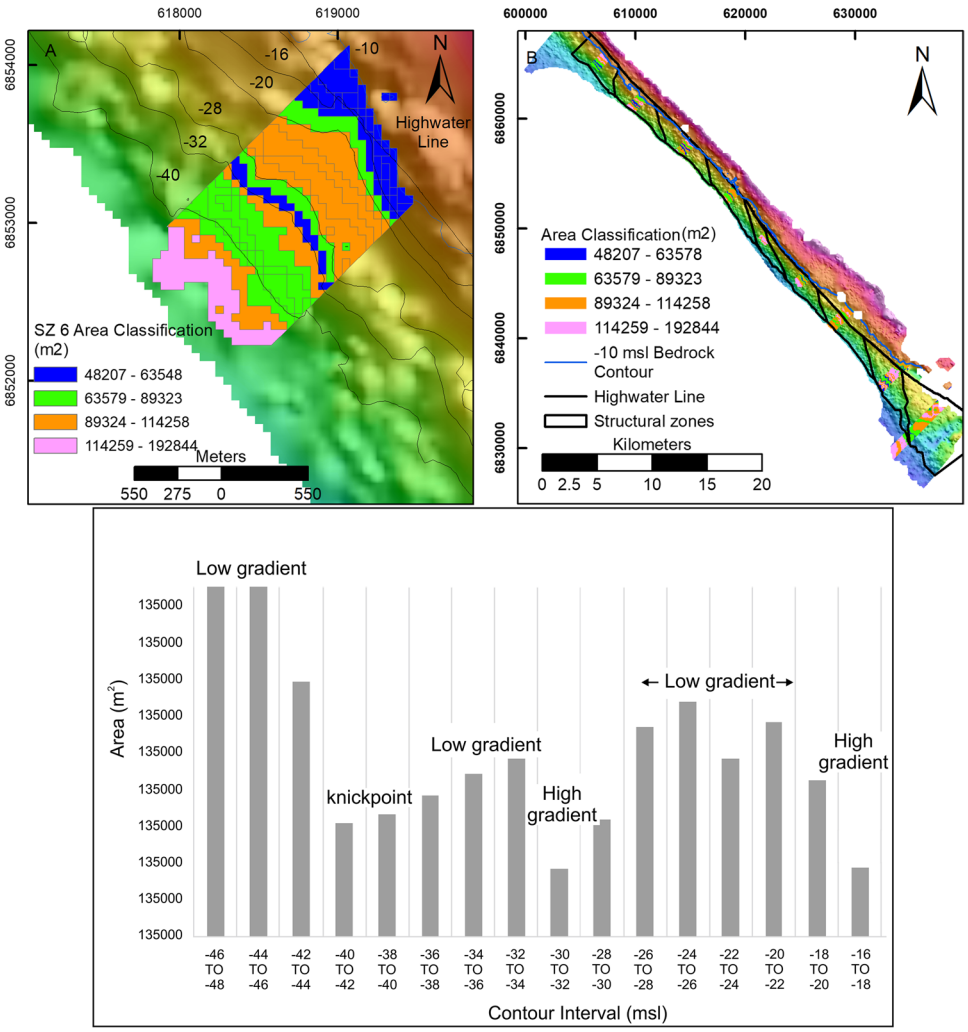

Fig. 9 **A** Example of 1-km-wide polygon classified by area per 2-m contour interval (after De Decker, 1987) within SZ6. **B** Overview map showing 1-km-wide polygons extracted from each structural zone. **C** Bar chart plot of the surface area analysis per 2-m contour interval for SZ6. Zones of increased surface area/low gradient and zones of decreased surface area/steeper gradient are annotated

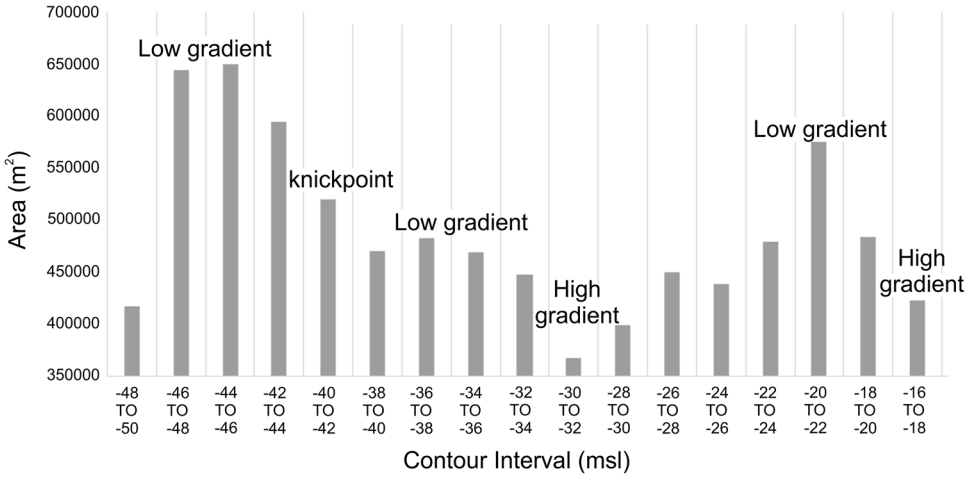

Fig. 10 Bar chart illustrating SZ4-9 area per 2-m contour interval analysis of 1-km-wide polygons. Zones of increased surface area/lower gradient and zones of lower surface area/steeper gradient are annotated

Fig. 10 shows the results of area per 2-m contour interval analysis for SZ 4–9 summed, between – 10 and – 50 msl. Note that not all zones have full coverage to depths of – 50 msl. The summed results are very similar to the example of SZ 6; a wider flatter interval between – 20 and – 22 msl is identified, preceded by a narrower, steeper interval between – 16 and – 20 msl. In the summed results, the area decreases and gradient steepens between – 24 and – 32 msl, with the steepest zone lying between – 28 and – 32 msl. Bedrock gradient flattens between – 34 and – 40 msl and then flattens significantly from – 40 msl to the edge of the dataset. These results agree with what has been visually interpreted in the seismic reflection data on a line-by-line basis (Fig. 4)

Multibeam bathymetry

The multibeam bathymetric surface (Fig. 11) was also subjected to the same analyses, and a 1-km-wide polygon subset of the data was extracted (Fig. 11B). A Natural Breaks (Jenks) classification of this dataset shows an inshore zone with the largest surface area per 2-m contour interval between – 20 and – 22 msl (pink), followed by a zone with slightly lower surface area (orange) between – 22 and – 28 msl. This is followed by the interval between – 28 and – 36 msl, which has the lowest surface area per contour interval (blue and yellow), i.e. the highest bedrock gradient zone. The surface area then increases for the interval between – 36 and – 38 msl. The plot of contour interval set against area is illustrated in Fig. 11C where the same broad trends derived from the bedrock elevation model can be seen.

Discussion

It remains widely acknowledged that locally, the high rugosity of the bedrock is the primary control on the extreme diamond grade variation that characterises this placer deposit (Jacob, 2016) and that at the macro scale, the bedrock gradient is controlled by a series of Neoproterozoic age, N-S trending faults (Kirkpatrick and Green, 2018). However, historical data collected during onshore mining operations also show that, onshore, the bedrock gradient, controlled by wave erosion on palaeo-rocky shorelines, is directly proportional to diamond grades at the scale relevant to practical resource estimation (Kirkpatrick et al., 2019b). It is hypothesised that during stillstands, mechanical, erosive forces of the waves concentrated by the long-lived microtidal range (~ 1.8 m) have, in conjunction with an abrasive bedload acting on a relatively softer bedrock, carved out a series of steep cliffs and associated low-gradient platforms (Fig.1 , Murray et al., 1970; Stocken, 1978; Trenhaile, 2000; Swantesson et al., 2006; Kennedy and Dickson, 2006; Trenhaile and Kanyaya, 2007, Stephenson and Naylor, 2011). Accurately mapping this scale of gradient variation offshore is required as a critical input for bankable resource estimation for the offshore extension of the deposit. However, it is a challenging task beneath a thick sediment overburden and against the backdrop of the high magnitude inherited structural gradient variation.

Offshore palaeo-shorelines derived from GIS analysis

As the structural features are Neo-Proterozoic to Cretaceous in age (Kirkpatrick and Green, 2018), the younger palaeo-shoreline expressions that we propose are evident in the data as coast-parallel gradient variations are superimposed on this regional, structural bedrock gradient control. These coast-parallel expressions are subtle when compared to the dominant N-S trending structural fabrics of the bedrock. We propose that the 'surface area per 2 m contour interval analysis' method applied along 1-km wide transects *within* structural zones, then averaged over

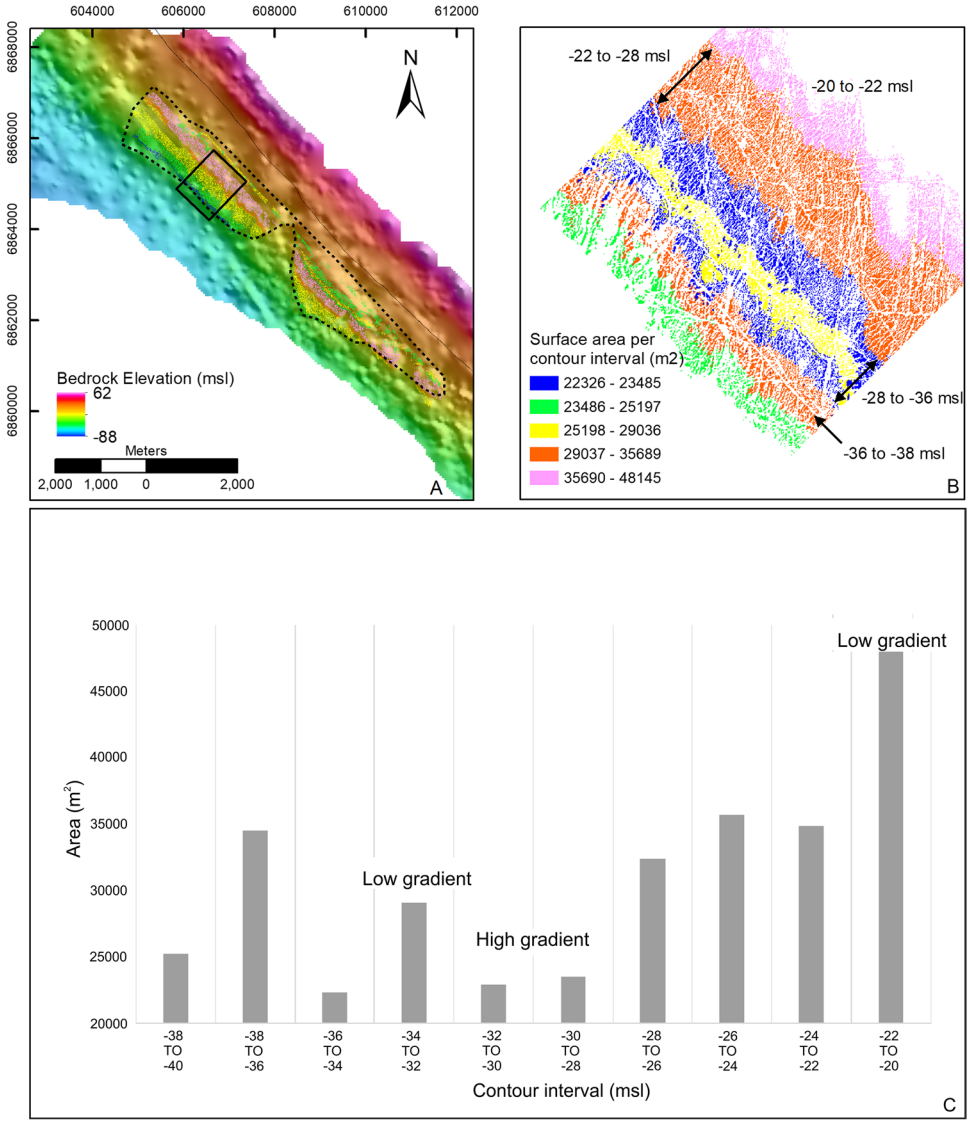

Fig. 11 Multibeam bathymetry bedrock surface area per contour interval analysis for 1-km-wide polygon. **A** The limited multibeam surface survey coverage with sediment infill removed (outlined by black dotted line) superimposed on the bedrock elevation surface. The 1-km-wide region used for the contour interval area analysis is shown by the black rectangle. **B** Inset polygon showing close-up of Natural Breaks (Jenks) classification of bedrock surface area per contour interval highlighting the − 28 to − 36 msl zone as a higher gradient zone. The colour scale depicts the classes of natural similarity as described in the text. **C** Bar chart plot of surface area per 2-m contour interval

the study area (Fig. 9), reveals trends in changes to the bedrock gradient, such that the small-scale topographic noise associated with the mapping of individual profiles is smoothed over, and a regional palaeo-shoreline picture appears (Fig. 10).

In the context of the detailed wave-cut platform and cliff morphology mapped historically onshore (Hallam 1964; Stocken 1978; Jacob et al. 2006), we suggest that the statistically inferred low-gradient zones (relatively higher surface area) be considered as regionally developed wave-cut platforms. These platforms are backed on the inshore by higher gradient zones (relatively lower surface area) within a 2- to 4-m elevation change or a distinct gradient knickpoint (Fig.10). These we interpret as micro-cliffs forming the retreating part of the upright portions of the rock coastal profile during platform development (c.f. Trenhaile, 1997, 2000).

Erosional palaeo-shorelines and palaeo-sea level constraints

Studies agree that a variety of factors interact to generate a site-specific wave-cut platform profile, e.g. lithology and rock resistances, availability and mobility of abrasive material, inherited morphology, structure, tidal range and length of time of sea level occupation at a specific elevation (Naylor et al. 2010; Trenhaile 2002; Dickson 2006; Blanco-Chao et al. 2007; Pérez-Alberti et al. 2012). Furthermore,

the relative interaction/importance of each of these factors undoubtedly changes over geological time to produce a unique shoreline.

In the context of southern Namibia, it is widely accepted that coarse sediments, intense wave energy to provide abrasive actions, focussed over the micro-tidal range, in conjunction with a receptive bedrock lithology (i.e. softer than abrasive agents) are the main factors contributing to the widespread formation of marine erosional (wave-cut) platforms (Jacob, 2001; Oelofsen, 2008). At present, the coast of southern Namibia is considered a soft coast, i.e. primarily depositional in nature (Naylor et al., 2010), and there are no other analogues for the erosional, extremely high sediment supply, high-energy southwestern Namibian coast of the past on the modern southern African coastline. That said, the sediment-free coastline to the north and south of the study area, in addition to bedrock exposed during mining operations close to MSL (Fig. 1), does provide some insight into the expected submerged platform morphology of the study area.

We consider older platforms, as observed in the raised bedrock underlying the onshore diamondiferous beaches (Fig., 1C), representative of the expected morphology of the entire schistose coastal tract from ~ − 55 to > 30 msl now covered in Holocene sediment. We do not have an exposed local modern analogue from which to constrain the elevation of platform development in relation to sea-level; however, a buried shore platform is evident between + 1 and − 1 m elevation from old exploration trench data (Fig. 1C). The current coastal areas are now inundated by sediment that blankets and obscures any shore platform that may form or have formed in the last few thousand years. However, studies recognise that on microtidal coasts mechanical wave erosion takes place through water hammer in the zone where air and water alternate, i.e. only in a narrow zone above and below fluctuating waterline (Trenhaile, 1997, 1999; Kennedy and Dickson, 2006; Porter et al., 2010).

Although abrasion by rock fragments, pebbles or sand is not as closely associated with the water level, its efficacy rapidly deceases below the waterline (Trenhaile, 1997), and most mathematical models suggest that waves also exert the greatest pressure at or slightly above the mean water surface (Martinez and Harbough, 1993). A study from an area of comparable wave energy and rock type in South Africa by Knight and Burningham (2019) similarly reveals contemporary shore platform elevations developed from 0 to + 3 m. Considering the above arguments, we therefore propose that wave-cut platforms in our study area form at elevations of between 0 and ~ + 2–3 m (as a landward limiting sea level index point, cf. Rovere et al., 2018).

Thebaudau et al. (2013) provide a comprehensive model of wave-cut platform evolution from the coast of Northern Ireland. Their results show that the contemporary rock platforms in the inter- to supratidal are likely to represent inheritance from multiple phases of sea level occupation. Taken as such, and in line with Trenhaile (2002), who notes that one of the most fundamental challenges in rock coast geomorphology is to determine the degree to which rock coasts are contemporary, rather than features inherited from the Quaternary, caution should be exercised in interpreting the erosional shorelines mapped from Oranjemund as strongly defined sea level data points. As argued by Thebaudau et al. (2013), the existence of, and relationship to, other regional shoreline features needs to be taken further into account. Despite the weak temporal control, the development of these erosional surfaces and possible multiple reactivation of them makes them attractive sites for resource upgrading due to prolonged focussing of wave energy. The following sections provide an analysis of each proposed shoreline in this light.

Submerged palaeo-shorelines on the southern coast of Namibia

Here, we outline the favourable comparison of, in particular, what we now call the − 20 m shoreline, to other more readily visually mapped palaeo-shorelines at this elevation, both on the southern African coastline and in other areas of similar GIA response. This lends significant confidence to our methodology in this geophysically challenging terrain.

The ~ − 20 msl shoreline

Figure 10 shows that the depth interval between − 20 and − 22 msl has an anomalously high surface area and is backed at its inshore side by a low surface area (high-gradient 4-m-high cliff) interval between − 16 and − 20 msl. The relationship of high-gradient to low-gradient zone at this elevation is reminiscent of that mapped by Murray et al. (1970) at equivalent depth between Mittag and Conception Bay north of the study area for over 550 km along shore. They recognised a submerged cliff with 1.5–5 m vertical relief that defined the landward edge of what they termed the '− 20 m platform' with variable widths and a slope of 1 in 70 (~ 0.36°).

South of the Orange River for ~ 100 km to Port Nolloth, historical bathymetry data from sediment-free zones (De Decker, 1987) show that the nearshore bedrock generally slopes down from the shore to ~ − 20 msl at an angle between 1.1 and 2°. Seawards, the seafloor levels out to a gradient of less than 0.5° to form the major part of the inner shelf between − 20 and − 40 msl. Up to 300 km north of our study area, Oelofsen (2008) used diamond size frequency distribution (SFD) data as a proxy for palaeo-shoreline positions. This study identified significant concentrations of diamonds between − 18 and − 21 msl.

Across areas of similar glacial isostatic adjustment (GIA) response (cf. Milne and Mitrovica, 2008), other shoreline features, mostly depositional, have also been reported. In South Africa, Ramsay (1996) identified a regional palaeo-shoreline on the east coast of South Africa from − 15 to − 25 m, from which a beachrock sample (− 17 m MSL) yielded a U-series data of 84,000 ± 3000 years BP. Cawthra et al. (2018) similarly reported a planation surface from the southern cape coast from − 15 to − 23 m, which was ascribed to MIS 5d.

− 28 to − 32 msl 'cliff'

Our analysis shows that the − 28 to − 32 msl interval is the most prominent zone of low surface area (high gradient) (Fig. 10) in the dataset. Seawards, between − 32 and − 40, the surface area analysis shows a slight flattening, followed by a marked flattening from − 40 msl (Fig.10). An increased slope at ~ − 30 msl was also recognized by Murray et al. (1970) in a sediment-free bathymetric profile just north of our study area. O'Shea (1971) reported anomalously flat bedrock at depths between − 32 and − 34 between Pomona and Dreimaster Bay (from Sparker profile analysis), which we now propose could be indicative of a wave-cut platform backed by a cliff as observed in our data.

Bastos et al. (2015) recognised a terrace at − 30 msl on the Abrolhos shelf of Brazil, and Gomes et al. (2020) similarly documented a 2-km-wide terrace at 30-m depth from the Rio Grande do Norte shelf. Cawthra et al. (2018) identified a palaeo-shoreline sequence at a depth of − 29 msl with a shallower erosional notch at − 28 msl and another notch to seaward at − 30 msl from the southern Cape coast of South Africa, which they considered MIS 5d in age. Engelbrecht et al. (2020) report a phase of Holocene delta construction to have marked a shoreline position at − 32 m on the east Coast of South Africa, which they ascribed to slowly rising sea levels from 10.1 to ≤ 9 cal kyr BP (Cooper et al., 2018a). Again, these match well with our observations.

− 40 msl platform

Figure 10 also shows a significant decrease in bedrock gradient from − 40 msl. De Decker (1987), Murray (1970) and O'Shea (1971) all record an extensively developed bedrock platform at this depth. The inshore boundary of our − 40 msl platform is, however, not marked by a prominent steepening of bedrock (i.e. cliff) as is the case for the − 20 msl and the − 32 msl platforms discussed above. Fig. 10 shows that rather this platform is merely bounded by a knickpoint marking a flattening of overall bedrock gradient.

On the shelf of southern Africa, there is much evidence for shoreline development and subsequent preservation at − 40 msl. Submerged coastal dune ridges are preserved off the coast of southern Mozambique (Wenau et al., 2020); aeolianite and preserved beach rock have been mapped off the east coast of South Africa (Green et al. 2013; 2014; 2020), and Cawthra et al. (2018) documented a palaeo-shoreline at − 40 msl on the southern coast of South Africa. Pretorius et al. (2016) recognise a prolonged sea level slowstand at 40-m depth, which has been ascribed to the development of flat erosional surfaces such as our − 40 msl shoreline.

Further afield, the Rio Grande do Norte shelf of Brazil also reveals a regionally developed terrace at − 40 m (Gomes et al., 2020), which was ascribed to the mid-Holocene period. Again, a similar depth pattern emerges in our new data set.

Bedrock morphology for diamond grade estimation philosophy

We consider the bedrock gradient changes that may be interpreted as wave-cut platforms and their associated backing cliffs or knickpoints to form in an overall steep coastal sector. This reflects Roy et al.'s (1994) model of transgression where steep slopes are linked to an "encroachment mode" of transgression. Here, the overall steep slope focuses on erosion due to the slow rates of recession, forming a flat profile to seaward of a landward migrating notch or cliff (see for example Cooper et al. (2018b) for a − 50 msl platform and cliff). This would compound any form of placer upgrading and thus the features mapped here contribute a significant advancement to the understanding of the regional grade variability, which is a critical component of resource estimation philosophy of the mining operation.

With regards timing, the exact genesis is unclear considering the variability in shoreline position when placed relative to commonly accepted glacio-eustatic sea level curves (Fig. 2). Given the small vertical uncertainty relative to modern shore platform formation on the southern Namibian margin (0- + 3 m MSL) and their clearly regional signatures for the coast of SW Africa, these seem to be good indicators of palaeo-sea level, though their temporal placement cannot be perfectly constrained. The best coincidence with glacio-eustatic sea level occupations is perhaps the time shortly after MIS 5c and the peak of MIS 5a for the − 30 msl shoreline (Fig. 2). The − 20 msl shoreline is less clear, but peaks in sea level at the MIS 5c mark are the best match for this. It seems unlikely that these can be ascribed to the MIS5d period as Cawthra et al. (2018) considered; sea level at this point was closer to − 60 msl and well out of the framework in which shore platforms have been considered to form in our study area.

The deepest shoreline, at − 40 msl, somewhat corresponds to the peak of MIS 5a. However, this depth is more recently associated with the slowstand of Pretorius et al. (2016) of between 10.8 to 10.6 ka (Cooper et al., 2018b). This is also

linked to a series of Holocene deltas that were constructed at – 40 msl on the high sediment supply Thukela margin (Engelbrecht et al., 2020) as well as high sedimentation rates recorded in the Orange River mudbelt south of the Orange River mouth between 11 and 9.2 ka (Herbert and Compton, 2007).

It is clear from the above arguments that the timing of similar shorelines developed around areas of similar GIA is diverse and inconsistent. This resonates with the findings of Rovere et al. (2018) that establishing a global sequence of drowned erosional shoreline features is a complicated and difficult task. As discussed by Thebaudau et al. (2013), it seems very likely that those features preserved on the Namibian shelf are composite features inherited from previous sea level states and reworked later by the last post-glacial transgression of MIS1. This makes their identification as sites of economic upgrading much more appealing, considering the composite lengths of reworking associated with these features (Compton et al., 2002; Kirkpatrick et al., 2019a).

Conclusions

Analysis of a dense, 200-m-spaced seismic reflection profile grid from the high sediment supply southwestern coastline of Namibia has reinforced the results of previous work, confirming that antecedent geology exhibits a first order control on the bedrock morphology of the region. However, within that context, onshore historical diamond data have also revealed that bedrock gradient changes related to wave erosion by the coarse bedload on coast-parallel, palaeo-rocky coast shorelines, during sea level stillstands or slow stands, act as important zones of economic upgrading of the diamondiferous bedload. Accurately identifying these shorelines is critical for resource estimation in the low grade, inherently variable and techno-economically challenging, nearshore placer diamond environment. This paper has demonstrated a GIS-based data analysis methodology that identifies bedrock gradient variations that we propose are indicative of these economically important erosional palaeo-shorelines against the backdrop of both the high, small-scale rugosity of the bedrock and the overarching antecedent structural control.

Low-gradient wave-cut platforms, backed by high-gradient cliff lines are interpreted at – 20 msl, – 32 msl and – 40 msl. These palaeo-shorelines are almost undoubtably composite features—a result of multiple sea level transgressions and regressions since the Eocene. However, comparison with areas of similar GIA response indicates that all three palaeo-shorelines were likely subject to focused wave action, and thus, economic upgrading of the diamondiferous bedload, during the latter part of MIS5 and the last transgression. We tentatively relate the latest phase of reworking and upgrading of the diamond placer deposit of the – 20 msl shoreline, to the peak of MIS 5c, the – 30 msl shoreline we relate to the time shortly after MIS 5c and the peak of MIS 5a. The deepest shoreline, at – 40 msl, we link to a period of slowstand between 10.8 and 10.6 ka.

Acknowledgements In particular, Dr J. Jacob are Mr G Grobbelaar are thanked for the support of the project. Mr L. Garlick and the Namdeb Survey Department as also thanked for the high-quality marine data acquisition. We also wish to thank Prof J. Compton, an anonymous reviewer, and the EiC, Prof Karin Bryan, for their insightful reviews and comments, which substantially improved this manuscript.

Funding This work was funded by the Mineral Resource Department of Namdeb Diamond Corporation (Pty) Ltd.

References

Aizawa M, Bluck BJ, Cartwright J, Milner S, Swart R, Ward J (2000) Constraints on the geomorphological evolution of Namibia from the offshore stratigraphic record. Commun Geol Surv Namibia 12:337–346

Bastos AC, Quaresma VS, Marangoni MB, D'Agostini DP, Bourguignon SN, Cetto PH, Silva AE, Amado Filho GM, Moura RL, Collins M (2015) Shelf morphology as an indicator of sedimentary regimes: a synthesis from a mixed siliciclastic-carbonate shelf on the eastern Brazil margin. J S Am Earth Sci 63:125–136

Bintanja R, van de Wal RSW (2008) North American ice-sheet dynamics and onset of 100,000-year glacial cycles. Nature 454:869–872

Blanco-Chao R, Pérez Alberti A, Trenhaile AS, Costa Casais M, Valcárcel Diaz M (2007) Shore platform abrasion in a para-periglacial environment, Galicia, northwestern Spain. Geomorphology 83:136–151

Bluck BJ, Ward JD, Spaggiari RI (2001) Gravel beaches of southern Namibia. In: Packham JR, Randall RE, Barnes RSK, Neal A (eds) Ecology and geomorphology of coastal shingle. Westbury Academic and Scientific Publishing, Otley, West Yorkshire, UK, pp 56–76

Bluck BJ, Ward JD, Cartwright J, Swart R (2007) The Orange River, southern Africa: an extreme example of a wave-dominated sediment dispersal system in the South Atlantic Ocean. J Geol Soc Lond 164:341–351

Corbett IB (1996) A review of diamondiferous marine deposits of western southern Africa. Afr Sci Rev 3:157–174

Corbett I, Burrell B (2001) The earliest Pleistocene (?) Orange River fan-delta: an example of successful exploration delivery aided by applied Quaternary research in diamond placer sedimentology and paleontology. Quat Int 82:63–73

Corvinus G (1983) The raised beaches of the West Coast of South West Africa/Namibia. Beck-Verlag, Munich, C.H, p 109

Cawthra HC, Jacobs Z, Compton JS, Fisher EC, Karkanas P, Marean CW (2018) Depositional and sea-level history from MIS 6 (Termination II) to MIS 3 on the southern continental shelf of South Africa. Quat Sci Rev 181:156–172

Compton JS, Mulabisana J, McMillan IK (2002) Origin and age of phosphorite from the Last Glacial Maximum to Holocene transgressive succession off the Orange River, South Africa. Mar Geol 186:243–261

Cooper JAG, Green AN, Compton JS (2018) Sea-level change in southern Africa since the Last Glacial Maximum. Quat Sci Rev 201:301–318

Cooper JAG, Meireles RP, Green AN, Klein AHF, Toldo EE (2018) Late Quaternary stratigraphic evolution of the inner continental shelf in response to sea-level change, Santa Catarina, Brazil. Mar Geol 297:1–24

Davis, RA, Clifton, HE, 1987. Sea-level change and the preservation potential of wave dominated and tide dominated coastal sequences. In: Nummedal, D, Pilkey, OH, Howard, JD (eds) Sea-level fluctuation and coastal evolution: SEPM Spec Pub 41: pp 167–178

Dickson ME (2006) Shore platform development around Lord Howe Island, southwest Pacific. Geomorphology 76:295–315

Dingle, RV, Siesser, WG, Newton, AR (1983) Mesozoic and Tertiary geology of Southern Africa. A.A. Balkema, Rotterdam 375 pp.

De Decker, RH (1987) The geological setting of diamondiferous deposits on the inner shelf between the Orange River and Wreck Point, Namaqualand. Bull Geol Surv S Afr 86.

Dingle RV, Hendey QB (1984) Late Mesozoic and Tertiary sediment supply to the eastern Cape Basin (SE Atlantic) and paleodrainage systems in southwestern Africa. Mar Geol 56:13–26

Engelbrecht L, Green AN, Cooper JAG, Hahn A, Zabel M, Mackay CF (2020) Construction and evolution of submerged deltaic bodies on the high energy SE African coastline: the interplay between relative sea level and antecedent controls. Mar Geol 424:106–170

Grant KM, Rohling EJ, Bronk Ramsay C, Cheng H, Edwards RL, Florindo F, Heslop D, Marra F, Roberts AP, Tamisiea ME, Williams F (2014) Sea-level variability over five glacial cycles. Nat Comms 5:5076

Green AN, Cooper JAG, Leuci R, Thackeray Z (2013) Formation and preservation of an overstepped segmented lagoon complex on a high-energy continental shelf. Sedimentology 60:1755–1768

Green AN, Cooper JAG, Salzmann L (2014) Geomorphic and stratigraphic signals of postglacial meltwater pulses on continental shelves. Geology 42:151–154

Green AN, Cooper, JAG., Dlamini, NP., Dladla, NP, Parker D, Kerwath, SE (2020) Relict and contemporary influences on the postglacial geomorphology and evolution of a current swept shelf: the Eastern Cape Coast, South Africa. Marine Geology 427: 106230

Gomes MP, Vital H, Droxler AW (2020) Terraces, reefs and valleys along the Brazil northeast outer shelf: deglacial sea-level archives. Geo-Mar Lett 40:699–711

Hallam CD (1964) The geology of the coastal diamond deposits of southern Africa (1959). In: Haughton, SH (ed) The geology of some ore deposits in Southern Africa, vol. 2. Geol Soc S Afr, pp. 671–729.

Hay, WW, Brock, JC (1992) Temporal variation in intensity of upwelling off southwest Africa. In: Summerhays, CP, Prell, WL, Emeis, KC (eds.) Upwelling systems: evolution since the Early Miocene. Geol Soc London Spec Pub 63, pp. 463–497.

Herbert CT (2009) Holocene sediment dynamics on the western margin of South Africa. PhD Thesis, University of Cape Town

Herbert CT, Compton JS (2007) Geochronology of Holocene sediments on the western margin of South Africa. S Afr J Geol 110:327–338

Hoyt JH, Oostdam BL, Smith DD (1969) Offshore sediments and valleys of the Orange River (South and South West Africa). Mar Geol 7:69–84

Jacob, RJ (2005) The erosional and Cenozoic depositional history of the lower Orange River, Southwestern Africa. PhD Thesis, University of Glasgow

Jacob J, Ward JD, Bluck BJ, Scholz RA, Frimmel HE (2006) Some observations on diamondiferous bedrock gully trapsites on Late Cainozoic, marine-cut platforms of the Sperrgebiet, Namibia. Ore Geol Rev 28:493–506

Jacob, J (2001) Late Proterozoic bedrock geology and its influence on Neogene marine diamondiferous trapsites, MA 1 - Sperrgebiet, Namibia. MSc Thesis, University of Cape Town.

Jacob, J (2016) Contextualized risk mitigation based on geological proxies in alluvial diamond mining using geostatistical techniques. Ph.D. Thesis. University of the Witwatersrand

Kennedy DM, Dickson ME (2007) Lithological control on the elevation of shore platforms in a microtidal setting. Earth Surf Process Landf 31:1575–1584

Lodewyks, T (2010) Seismic stratigraphy of upper Pleistocene gravel and Holocene mudbelt deposits between wreck point and the Kamma River on the western shelf of South Africa. MSc thesis University of Cape Town

Kirkpatrick LH, Green AN (2018) Antecedent geologic control on nearshore morphological development: the wave dominated high sediment supply shoreface of southern Namibia. Mar Geol 403:34–47

Kirkpatrick LH, Green AN, Pether J (201AD) The seismic stratigraphy of the inner shelf of southern Namibia: the development of an unusual nearshore shelf stratigraphy. Mar Geol 408C:18–35

Kirkpatrick LH, Jacob J, Green AN (2019) Beaches and bedrock: how geological framework controls coastal morphology and the relative grade of a Southern Namibian diamond placer deposit. Ore Geol Rev 107:853–862

Knight J, Burningham H (2019) Bedrock hardness values and morphological zonation of a shore platform in South Africa. Trans Royal Soc S Afr 75:40–53

Matsumoto H, Dickson ME, Kench PS (2016a) An exploratory numerical model of rocky shore profile evolution. Geomorphology 268:98–109

Matsumoto, H, Dickson, ME, Kench, PS (2016b) Modelling the development of varied shore profile geometry on rocky coasts. J Coastal Res SI175: 597–601.

Milne GA, Mitrovica JX (2008) Searching for eustacy in de-glacial sea-level histories. Quat Sci Rev 27:2292–2302

Martinez PA, Harbaugh JW (1993) Simulating nearshore environments. Pergamom Press Limited, Headyton Hill Hall, Oxford

Murray, LG, Joynt, RH, O'Shea, DOC., Foster, RW., Kleinjan, L (1970) The geological environment of some diamond deposits off the coast of South West Africa. In: Delany, FM (ed) The geology of the east Atlantic continental margin. Rep. Inst. Geol. Sci., 70: pp 119–141.

Nakashole AN, Hodgson DM, Chapman RJ, Morgan DJ, Jacob RJ (2018) Long-term controls on continental-scale bedrock river terrace deposition from integrated clast and heavy mineral assemblage analysis: an example for the lower Orange River, Namibia. Sed Geol 364:103–120

Naylor LA, Stephenson WJ, Trenhaile AS (2010) Rock coast geomorphology: recent advances and future research directions. Geomorphology 114:3–11

Naylor LA, Coombes MA, Viles HA (2012) Reconceptualising the role of organisms in the erosion of rock coasts: a new model. Geomorphology 157–158:17–30

Oosterveld, MM, Campbell, D, Hazell, KR (1987) Geology related to statistical evaluation parameters for a diamondiferous beach deposit. Proceedings of the 20th International Symposium on the Application of Computers and Mathematics in the Mineral Industries Geostatistics: 3, pp. 129–136.

Oelofsen, A (2008) Late Cainozoic shallow marine diamond placers off the northern Sperrgebiet, Namibia. MSc thesis University of Cape Town

O'Shea, DOC (1971) An outline of the inshore submarine geology of southern S.W.A. and Namaqualand MSC thesis University of Cape Town

Pether J (1986) Late Tertiary and early Quaternary marine deposits of the Namaqualand Coast, Cape Province: new perspectives. S Afr J Sci 82:464–470

Pérez-Alberti A, Trenhaile AS, Pires A, López-Bodoya J, Chaminé H, Gomes A (2012) The effect of boulders on shore platform development and morphology in Galicia, north west Spain. Cont Shelf Res 48:122–137

Pretorius L, Green AN, Cooper JAG (2016) Submerged shoreline preservation and ravinement during rapid postglacial sea-level rise and subsequent "slowstand." Geol Soc Am Bull 128:1059–1069

Prins CF, Jacob J (2014) Improved variography using simulated annealing to adjust sample locations to align with diamondiferous linear beach structures. J Southern Afr Inst Mining Metall 114:1–3

Porter NJ, Trenhaile AS, Prestanski KJ, Kanyaya JI (2010) Shore platform downwearing in eastern Canada: micro-tidal Gaspé, Québec. Geomorphology 116:77–86

Ramsay PJ (1996) 9000 years of sea-level change along the southern African coastline. Quat Int 31:71–75

Rau G (2003) The integrated use of detailed geophysical, geological and oceanographic techniques to delineate and prioritise marine diamond placer deposits on the Inner Shelf, West Coast, Central Namibia: EPL 1950 (Hottentot Bay) – A Case Study. MSc Thesis Rhodes University

Rogers, J (1977) Sedimentation on the continental margin off the Orange River and the Namib Desert Mar Geosci Group Bull 7: 162 p.

Rovere A, Khanna P, Bianchi CN, Droxler AW, Morri C, Naar DF (2018) Submerged reef terraces in the Maldivian Archipelago (Indian Ocean). Geomorphology 317:218–232

Roy PS, Cowell PJ, Ferland MA, Thom BG (1994) Wave-dominated coasts. In: Carter RWG, Woodruffe CD (eds) Coastal evolution: late Quaternary shoreline morphodynamics. Cambridge University Press, Cambridge, p 121p

Runds MJ, Bordy EM, Pether J (2019) Late Quaternary sedimentological history of a submerged gravel barrier beach complex, southern Namibia. Geo-Mar Lett 39:469–491

Stephenson WJ, Naylor LA (2011) Geological controls on boulder protection in a rock coast setting: insights from South Wales, U.K. Mar Geo 283:12–24

Stephenson WJ, Dickson ME, Denys PH (2017) New insights on the relative contributions of coastal processes and tectonics to shore development following the Kaikōura earthquake. Earth Surf Process Landf 42:2214–2220

Stevenson IR, McMillan IK (2004) Incised valley fill stratigraphy of the Upper Cretaceous succession, proximal Orange Basin, Atlantic margin of southern Africa. J Geol Soc Lond 161:185–208

Stocken, C.G., 1978. A review of the later Mesozoic and Cenozoic deposits of the Sperrgebiet. Unpublished Report, Consolidated Diamond Mines of South West Africa (Pty.) Ltd. 38 pp.

Swantesson JOH, Gómex-Pujol L, Cruslock EM, Fornoós JJ, Balaguer P (2006) Processes and patterns of erosion and downwearing on micro-tidal rock coasts in Sweden and the western Mediterranean. European Shore Platform Dynamics. Zeits Für Geomorph 144:137–160

Trenhaile AS (1999) The width of shore platforms in Britain, Canada and Japan. J Coast Res 15:355–364

Trenhaile AS (1997) Coastal dynamics and landforms. Oxford University Press, Oxford

Trenhaile AS (2000) Modeling the development of wave-cut shore platforms. Mar Geo 166:163–178

Trenhaile AS (2002) Modeling the development of marine terraces on tectonically mobile rock coasts. Mar Geol 185:341–361

Trenhaile AS (2005) Modelling the effect of waves, weathering and beach development on the shore platform development. Earth Surf Process Landf 30:613–634

Trenhaile AS (2008) Modeling the role of weathering in shore platform development. Geomorphology 94:24–39

Trenhaile AS (2010) The effect of Holocene changes in relative sea level on the morphology of rocky coasts. Geomorphology 114:30–41

Trenhaile AS (2016) Rocky coasts – their role as depositional environments. Earth Sci Rev 159:1–13

Trenhaile AS, Kanyaya JI (2007) The role of wave erosion on sloping and horizontal shore platforms in macro-and mesotidal environments. Journ Coast Res 23:298–309

Thébaudeau B, Trenhaile AS, Edwards RJ (2013) Modelling the development of rocky shoreline profiles along the northern coast of Ireland. Geomorphology 203:66–78

Ward, JD, Bluck, BJ (1997) The Orange River – 100 million years of fluvial evolution in southern Africa. Abstracts volume of the 6th International Fluvial Conference. Cape Town: International Association of Sedimentologists.

Wenau S, Preu B, Spiess V (2020) Geological development of the Limpopo Shelf (southern Mozambique) during the last sea level cycle. Geo-Mar Lett 40:363–377